

## YOHKOH SXT FULL-RESOLUTION OBSERVATIONS OF SIGMOIDS: STRUCTURE, FORMATION, AND ERUPTION

RICHARD C. CANFIELD,<sup>1</sup> MARIA D. KAZACHENKO,<sup>1</sup> LOREN W. ACTON,<sup>1</sup> D. H. MACKAY,<sup>2</sup> JI SON,<sup>3</sup> AND TANYA L. FREEMAN<sup>4</sup>

Received 2007 July 31; accepted 2007 October 19; published 2007 November 13

### ABSTRACT

We study the structure of 107 bright sigmoids using full-resolution (2.5'' pixels) images from the *Yohkoh* Soft X-Ray Telescope (SXT) obtained between 1991 December and 2001 December. We find that none of these sigmoids are made of single loops of S or inverse-S shape; all comprise a pattern of multiple loops. We also find that all S-shaped sigmoids are made of right-bearing loops and all inverse-S-shaped sigmoids of left-bearing loops, without exception. We co-align the SXT images with Kitt Peak magnetograms to determine the magnetic field directions in each sigmoid. We use a potential-field source surface model to determine the direction of the overlying magnetic field. We find that sigmoids for which the relative orientation of these two fields has a parallel component outnumber antiparallel ones by more than an order of magnitude. We find that the number of sigmoids per active region varies with the solar cycle in a manner that is consistent with this finding. Finally, those few sigmoids that are antiparallel erupt roughly twice as often as those that are parallel. We briefly discuss the implications of these results in terms of formation and eruption mechanisms of flux tubes and sigmoids.

*Subject headings:* Sun: activity — Sun: magnetic fields

*Online material:* color figure

### 1. INTRODUCTION

Sinuuous (sigmoidal) structures linking neighboring active regions (ARs) were noted by Acton et al. (1992) in images made using the *Yohkoh* Soft X-Ray Telescope (SXT; Tsuneta et al. 1991). However, the S or inverse-S structures now commonly called sigmoids occur within ARs, not between them, are often accompanied by H $\alpha$  filaments, and are thought to be manifestations of magnetic flux ropes embedded in the solar corona (Gibson et al. 2006). They brighten in association with eruptions and long-duration flares (Rust & Kumar 1996) and participate in a transition from sigmoid to arcade morphology over a time frame spanning an eruption (Sterling & Hudson 1997; Hudson et al. 1998). The statistically significant demonstration that active regions are more likely to be eruptive if they are either sigmoidal or large (Canfield et al. 1999) has led to interest in sigmoids as precursors of solar eruptions (Canfield et al. 2000).

A topological model consisting of a twisted flux rope embedded in a surrounding field (e.g., Titov & Démoulin 1999) can explain the shape and brightness of X-ray sigmoids. A flux rope model can also explain many interplanetary magnetic clouds associated with the eruption of sigmoids (Leamon et al. 2002). Given that magnetic helicity is a well-conserved quantity under coronal circumstances (Berger 1984; Brown et al. 1999), it is tempting to associate the helical structure underlying sigmoids with magnetic clouds. However, Leamon et al. (2002) showed that there is no consistent relationship between either the flux content or handedness of magnetic clouds and the flux content or handedness of the solar active regions with which they are associated. They concluded that this implicates reconnection of the AR with its surroundings. One would expect that if such reconnection is to take place, relative orientation

is important. This motivates our study of the orientation of sigmoids with respect to the magnetic fields overlying them.

### 2. INSTRUMENTATION AND DATA

In this study we use the highest resolution imaging mode of the *Yohkoh* SXT, whose basic element is a  $1 \times 1$  partial frame image (PFI), an array of  $64 \times 64$  pixels of  $2.5'' \times 2.5''$  size. The *Yohkoh* Legacy Archive<sup>5</sup> provides both PFIs and lower resolution full-disk images. The standard SXT observing program typically used the PFI mode to observe either the site identified by the spacecraft flare flag (the flare mode) or the brightest site on the solar disk (the quiet mode).

We have identified all ARs observed with PFIs over the *Yohkoh* mission that unambiguously show S or inverse-S form; this data set comprises 107 sigmoids. Of course, their occurrence rate varies with the sunspot number over the 1991–2001 mission, which spanned three distinctive cycle phases (Dikpati et al. 2004): (1) 12/91–07/96, most of the declining phase of Cycle 22; (2) 08/96–07/00, all of the rising phase of Cycle 23; (3) 08/00–12/01, the first 16 months of the declining phase of Cycle 23. We focus on more subtle variations below.

Magnetograms from the Kitt Peak Vacuum Telescope (KPVT), which we obtained from the NSO/KP Vacuum Telescope ftp archive,<sup>6</sup> played two roles in our study. First, the KPVT full-disk photospheric (868.8 nm) FITS-format magnetograms, whose spatial resolution (pixel size) was  $\sim 1.0''$  before 1993,  $\sim 1.14''$  thereafter, were co-aligned with SXT images to determine the magnetic field direction in individual loops. Second, the KPVT low-resolution ( $360 \times 180$ ) synoptic photospheric magnetograms were used to generate potential field source-surface models of the coronal magnetic field, in order to determine the direction of the magnetic field overlying the sigmoid of interest.

<sup>1</sup> Physics Department, Montana State University, Bozeman, MT 59717.

<sup>2</sup> School of Mathematics and Statistics, University of Saint Andrews, Saint Andrews, Fife KY16 9SS, Scotland.

<sup>3</sup> Departments of Aerospace Engineering and Physics, University of California, Irvine, CA 92697.

<sup>4</sup> Division of Sciences, Union College, Lincoln, NE 68506.

<sup>5</sup> See <http://solar.physics.montana.edu/ylegacy>.

<sup>6</sup> See <http://nsokp.nso.edu/dataarch.html>.

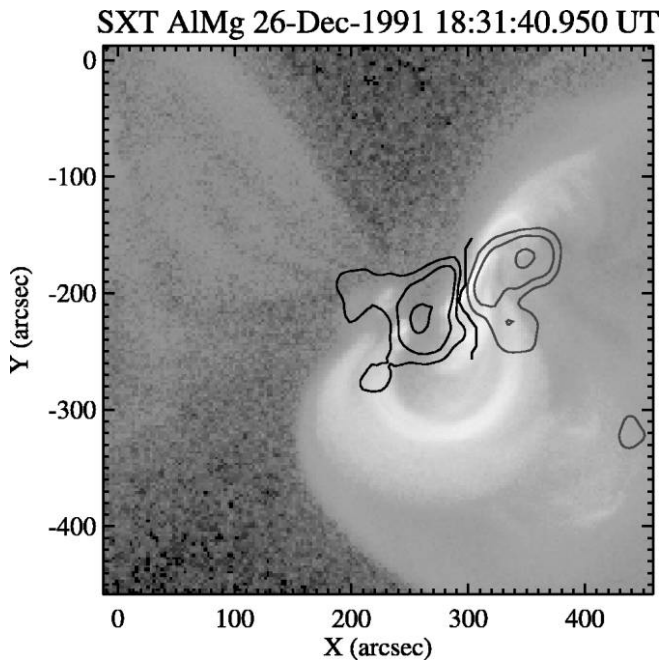


FIG. 1.—Co-aligned overlay of an SXT PFI image of the forward-S sigmoid in NOAA AR 6982, 1991 December 26 18:32 UT, on magnetic field contours from the KPVT magnetogram of TBD UT, 1991 December 26, after correction for the UT difference and differential rotation. X and Y coordinates are relative to disk center. Red (black) contours indicate positive (negative) magnetic flux. Contour levels are 200, 400, and 800 G. The polarity inversion line is shown in heavier black. No single loop defines the forward-S shape; it is a pattern. Loops in the central region are right-bearing. [See the electronic edition of the *Journal* for a color version of this figure.]

### 3. OBSERVATIONS, ANALYSIS AND RESULTS

#### 3.1. Internal Structure and Skew

Figure 1 shows a PFI image of the first of the 107 sigmoids, which occurred in NOAA AR 6982, at Carrington longitude  $142^\circ$  and latitude  $-14^\circ$ . This sigmoid comprises a pattern of many loops. It is typical in that respect: *none of the 107 sigmoids in our study have an S or inverse-S shape that is defined by a single loop.*

The skew of the individual loops with respect to the S-shaped axis of the sigmoid (whose central axis typically lies along the photospheric polarity inversion line) is an observable parameter of the pattern. In this work we describe the skew of loops relative to the sigmoid axis in the customary manner: right-bearing (R) or left-bearing (L), in analogy with exit ramps from a highway. We determine the skew from those loops that are midway between the sigmoid’s upper and lower elbows (in the terminology of Moore et al. 2001). For example, the loops of the S-shaped sigmoid in Figure 1 are right-bearing. We have determined the skew of the loops comprising all sigmoids in our study. For every one of our 107 observed sigmoids, there is a one-to-one relationship between the shape of the sigmoid and the skew of the loops: *all S-shaped sigmoids are made of right-bearing loops and all inverse-S-shaped sigmoids of left-bearing loops.*

To better understand the interaction of our sigmoids with their surroundings, we need not just the skew, but the actual magnetic field direction, along the individual loops that comprise each of the listed sigmoids. We therefore co-align full-disk SXT images with cotemporal full-disk Kitt Peak magnetograms at the nearest times at which the latter are available. Figure 1 shows an overlay of the sigmoid in NOAA AR 6982

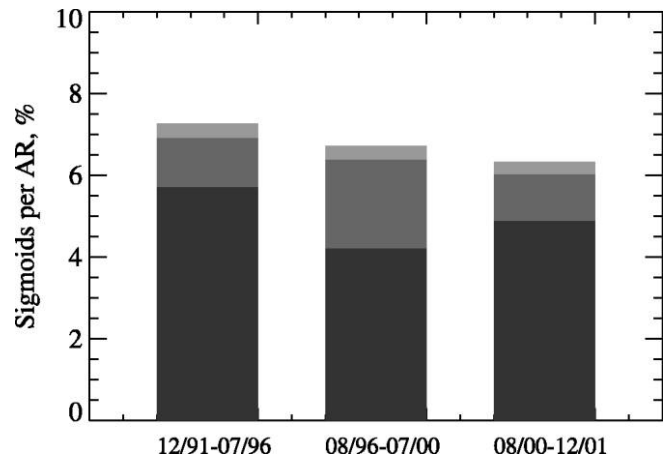


FIG. 2.—Observed distributions of relative orientations of sigmoids (per PFI-observed AR) with respect to the overlying coronal field at three phases of the solar cycle: Cycle 22 declining phase (left), comprising 42 sigmoids; Cycle 23 rising phase (center), comprising 43 sigmoids; Cycle 23 declining phase (right), comprising 22 sigmoids. Gray scale for relative orientation bins defined in § 3.2: black: parallel; dark gray: perpendicular; light gray: antiparallel.

using such co-alignment. Overlays such as that shown in Figure 1 allow us to assign a magnetic field direction to each of the observed loops. The field in the loops that comprise this sigmoid emerge on the western side of the polarity inversion line (PIL) and arch over it in a southeasterly direction. For later comparison with overlying fields in § 3.2, we determine the magnetic field direction in the observed loops in the central part of the sigmoid, between the elbows. We call this its “sigmoid field direction” below. Of course, the magnetic fields of a given sigmoid at its interface with the overlying field must span a substantial range of directions. Although this single value is therefore approximate, it is representative, observable, reproducible, and model-independent.

#### 3.2. Orientation Relative to Overlying Magnetic Fields

To determine the direction of magnetic fields in the corona above the upper boundary of the observed sigmoids, we use the potential-field source-surface (PFSS) model of van Ballegoijen et al. (1998) and NSO/KP Vacuum Telescope synoptic magnetograms. Assuming a source surface at  $2.5 R_\odot$ , we extrapolate spherical harmonics of the observed photospheric magnetic field.

We determine the lowest height at which no field lines close within the AR that harbors the sigmoid (typically the immediately overlying field lines connect down to polar boundary regions). We then determine the “overlying field direction” above the PIL at this height (which is typically  $0.4\text{--}0.8 R_\odot$  above the photosphere).

Having determined both the sigmoid field direction and the overlying field direction for all 107 sigmoids, we determine their relative orientation values and sort them into three bins: parallel within  $\pm 60^\circ$ , perpendicular within  $\pm 30^\circ$ , and antiparallel within  $\pm 60^\circ$ . The  $\pm 30^\circ$  width of the perpendicular bin is our estimate of the uncertainty of the relative orientation values due to measurement error. Hence, appearance of a given sigmoid in either the parallel or antiparallel bin means that the relative orientation of the sigmoid and its overlying field has a significant parallel or antiparallel component. We use the concise terminology “parallel or antiparallel sigmoid” in this sense below.

Figure 2 shows the distribution of relative orientation values

in these bins during the three solar cycle phases of the *Yohkoh* mission defined in § 2. If the distribution of orientations was random, the number of sigmoids in the parallel and antiparallel bins (*black and light gray, respectively*) would be equal, and the number in the perpendicular bin would be half as large as the others. In fact, summing over all three cycle periods, orientations with a parallel component are more than an order of magnitude more common than antiparallel. Applying the  $\chi^2$  test (Daniel 1990) to the data shown in Figure 2, we find that the probability that orientation is randomly distributed is less than  $10^{-5}$ . We conclude that *sigmoid magnetic fields strongly tend to have a component that is parallel to the coronal magnetic fields that overlie them*.

### 3.3. Solar Cycle Dependences

Of course, we expect the number of sigmoids to vary with the solar cycle simply because the number of ARs does so. More subtle solar cycle dependences are present in our observations. The most apparent is found in the distribution of relative orientations shown in Figure 2. Contrasting the rising phase of Cycle 23 with the two declining phase samples, the percentage of sigmoids in the perpendicular bin is noticeably larger and in the parallel bin smaller.

According to the  $\chi^2$  test, the probability that the Cycle 23 rising phase sample in Figure 2 is drawn from a population characterized by the Cycle 22 declining phase distribution in the same figure is only about 2%, while the probability that the Cycle 23 declining phase sample is drawn from a population given by the Cycle 22 declining phase distribution is over 99%. Hence, we conclude that *the difference between the rising and declining phase distributions of relative orientations is real*.

We find no reason to believe that PFI selection effects significantly bias these distributions. Comparing the Cycle 22 declining phase to the Cycle 23 rising phase, the fraction of all ARs on the solar disk that are sampled with PFIs is virtually identical at 58%. During the declining phase of Cycle 23, the fraction is only slightly different at 53%.

Figure 3 shows how a solar cycle variation in the relative orientation between sigmoid fields and global solar dipole fields arises. The polar and AR region magnetic polarities are appropriate for Cycles 22 and 23 (Dikpati et al. 2004). The hemispheric trend of AR region handedness (labeled LH, RH) (Pevtsov et al. 1995) does not vary with the solar cycle (Pevtsov et al. 2001). The dashed lines indicate polarity inversion lines along which sigmoids typically lie (see, e.g., Fig. 1). The sigmoid in this figure is typical; it has an S shape and right-bearing skew, which corresponds to RH twist in a flux rope interpretation (Titov & Démoulin 1999). The arrows in Figure 3 indicate that the expected field direction for this sigmoid is toward the southeast, as observed in Figure 1. As the trends in Figure 3 show, the solar cycle sequence for the relative orientation of sigmoid and overlying fields is parallel, antiparallel, and parallel, respectively, during the three periods shown in Figure 2. Hence, the observed solar cycle variation of the number of parallel, perpendicular, and antiparallel sigmoids in Figure 2 is consistent with the result of § 3.2 that sigmoids occur primarily in the parallel relative orientation.

### 3.4. Eruptions

We now turn to observational signatures of eruption. Because no white-light coronagraphs were in orbit during the first half of the *Yohkoh* mission, we use two well-documented proxies for coronal mass ejections (CMEs), postflare cusps and arcades

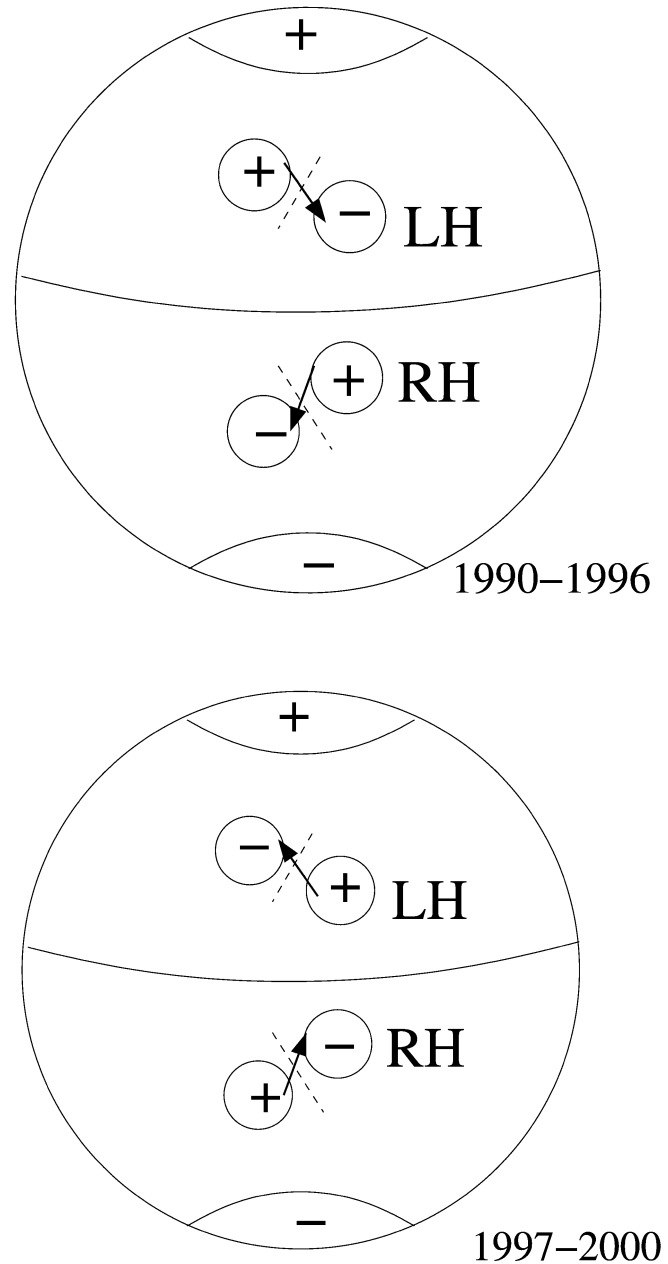


FIG. 3.—Solar cycle dependence of expected sigmoid loop directions relative to large-scale dipole for Cycle 22 declining phase (*top*) and Cycle 23 rising phase (*bottom*). The Cycle 23 declining phase is the same as the top panel, but with all arrows and poles reversed. See discussion in § 3.3.

(Sterling & Hudson 1997; Hudson et al. 1998) as well as direct SXT observation of moving ejecta. We have evaluated these proxies during the second half of the *Yohkoh* mission, when CMEs were observed with the white-light coronagraph (LASCO) aboard the *SOHO* mission (Brueckner et al. 1995). From this evaluation, using moving ejecta, arcades, and cusps over  $10^\circ$  (heliographic) span at their base as our proxies, we found that 83% of the eruptions we identified were listed as CMEs in the LASCO catalog.

Both the frequency and solar cycle distribution of sigmoid eruptions are of interest. Using the proxies just discussed, we have determined the number of eruptions  $N_e$  from sigmoids in each orientation and solar cycle bin. We have then determined the number of days between the first and last appearance of

the sigmoids in the full-disk SXT data—the number of days  $N_d$  the sigmoids are visible. The distribution of  $N_e$  over  $N_d$  is shown in Figure 4. Over the whole mission, the number of eruptions per sigmoid per day is about a factor of 2 greater for antiparallel sigmoids than parallel ones.

Also, we find a strong solar cycle dependence. According to the  $\chi^2$  test, the hypothesis that the Cycle 23 rising phase distribution of  $N_e$  is consistent with that of the Cycle 22 declining phase has a probability of less than  $10^{-5}$ . On the other hand, the hypothesis that Cycle 23 is described by the Cycle 22 distribution has a probability of 10%, which is not statistically compelling.

#### 4. SUMMARY AND CONCLUSIONS

We find that at *Yohkoh* SXT full resolution (2.5" pixels), all of the 107 clearly defined sigmoids observed throughout the mission are composed of multiple loops. None have an S or inverse-S shape that is defined by a single loop. The skew of the loops that comprise these sigmoids bears a systematic relationship to the shape, without significant exception. All S-shaped sigmoids are made of right-bearing loops and all inverse-S-shaped sigmoids of left-bearing loops. These properties strongly support the notion that X-rays from sigmoids originate at the interface between twisted flux ropes and their surroundings (Titov & Démoulin 1999).

We find that magnetic field directions in the overwhelming majority of sigmoids have a component that parallels those of the overlying magnetic fields; such parallel sigmoids outnumber antiparallel ones by more than an order of magnitude. The solar cycle variation of sigmoids is consistent with this finding. More sigmoids, and particularly more parallel sigmoids, are found per AR region during the declining phases of Cycles 22 and 23 than during the rising phase of Cycle 23. These properties support two alternative interpretations. The first alternative is that reconnection of ARs regions with the fields that overlie them prevents flux ropes from forming. This process was seen in the simulations of Fan & Gibson (2004), who modeled the emergence of pre-existing flux ropes into an overlying coronal arcade. They found that in the antiparallel configuration, the flux rope reconnected with the arcade field almost as soon as it emerged. The second alternative is that the formation of flux ropes takes place by reconnection in a sheared arcade (van Ballegoijen & Martens 1989; Mackay & van Ballegoijen 2006). In this process the azimuthal component of the upper boundary field direction is invariably parallel to the field just above it.

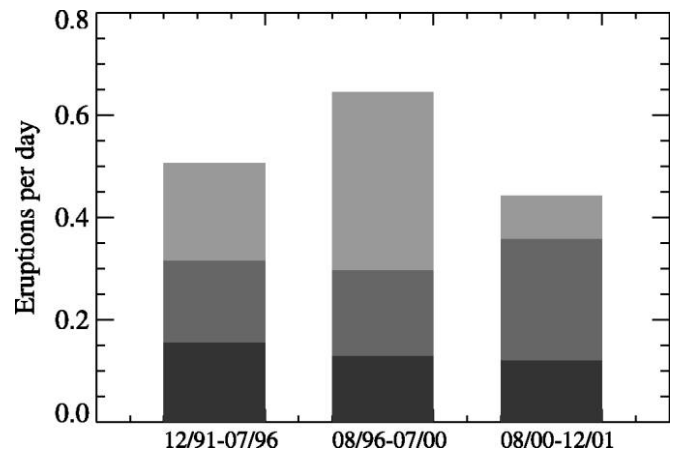


FIG. 4.—Dependence of frequency of eruption of observed sigmoids on relative orientation of the sigmoid and the overlying field for Cycle 22 declining phase (left), 68 eruptions; Cycle 23 rising phase (center), 72 eruptions; Cycle 23 declining phase (right), 31 eruptions. Black: parallel; dark gray: perpendicular; light gray: antiparallel, as in Fig. 2. See discussion in § 3.4.

Those unusual sigmoids whose field direction is antiparallel with respect to the overlying field erupt about twice as often per sigmoid as those that are parallel. This is an indication that breakout reconnection (Antiochos 1998) plays a role. However, an order of magnitude more sigmoids are found in the parallel orientation, so such sigmoids account for far more eruptions than antiparallel ones. On the other hand, there is ample observational support for the runaway tether cutting model in the sigmoid eruptions studied by Moore et al. (2001). Although this process for eruption may be less efficient than breakout, our results imply that the much larger population of parallel sigmoids makes it the most likely mechanism for the large majority of sigmoid eruptions.

The authors thank the referee, whose report significantly improved the manuscript. We gratefully acknowledge support from NASA through LWS grant NNG05-GJ96G (R. C. C., M. K.) and NSF through REU grant ATM-0243923 (J. S., T. L. F.). Creation of the *Yohkoh* Legacy Archive was supported by NASA/GSFC under grants NNG04O33G and NNG06GA49G. We thank Aki Takeda for creating the fully corrected PFIs. The development of the NSO Digital Library has been generously supported by the National Science Foundation through its National Space Weather Program, and by NASA under the Upper Atmosphere Research Program.

#### REFERENCES

- Acton, L., et al. 1992, *Science*, 258, 618  
 Antiochos, S. K. 1998, *ApJ*, 502, L181  
 Berger, M. A. 1984, *Geophys. Astrophys. Fluid Dyn.*, 30, 79  
 Brown, M. R., Canfield, R. C., & Pevtsov, A. A. 1999, *Magnetic Helicity in Space and Laboratory Plasmas* (Washington, DC: AGU)  
 Brueckner, G. E., et al. 1995, *Sol. Phys.*, 162, 357  
 Canfield, R. C., Hudson, H. S., & McKenzie, D. E. 1999, *Geophys. Res. Lett.*, 26, 627  
 Canfield, R. C., Hudson, H. S., & Pevtsov, A. A. 2000, *IEEE Transactions on Plasma Science*, 1786  
 Daniel, W. W. 1990, *Applied Nonparametric Statistics* (2nd. ed.; Boston: PWS-KENT)  
 Dikpati, M., de Toma, G., Gilman, P. A., Arge, C. N., & White, O. R. 2004, *ApJ*, 601, 1136  
 Fan, Y., & Gibson, S. E. 2004, *ApJ*, 609, 1123  
 Gibson, S. E., Fan, Y., Török, T., & Kliem, B. 2006, *Space Sci. Rev.*, 124, 131  
 Hudson, H. S., Lemen, J. R., St. Cyr, O. C., Sterling, A. C., & Webb, D. F. 1998, *Geophys. Res. Lett.*, 25, 2481  
 Leamon, R. J., Canfield, R. C., & Pevtsov, A. A. 2002, *J. Geophys. Res.*, 107, 1234  
 Mackay, D. H., & van Ballegoijen, A. A. 2006, *ApJ*, 641, 577  
 Moore, R. L., Sterling, A. C., Hudson, H. S., & Lemen, J. R. 2001, *ApJ*, 552, 833  
 Pevtsov, A. A., Canfield, R. C., & Latushko, S. M. 2001, *ApJ*, 549, L261  
 Pevtsov, A. A., Canfield, R. C., & Metcalf, T. R. 1995, *ApJ*, 440, L109  
 Rust, D. M., & Kumar, A. 1996, *ApJ*, 464, L199  
 Sterling, A. C., & Hudson, H. S. 1997, *ApJ*, 491, L55  
 Titov, V. S., & Démoulin, P. 1999, *A&A*, 351, 707  
 Tsuneta, S., et al. 1991, *Sol. Phys.*, 136, 37  
 van Ballegoijen, A. A., Cartledge, N. P., & Priest, E. R. 1998, *ApJ*, 501, 866  
 van Ballegoijen, A. A., & Martens, P. C. H. 1989, *ApJ*, 343, 971